THE UNVERSITY OF TULSA

WELLBORE STABILITY ANALYSIS

ADVANCED DRILLING ENGINEERING PROJECT

Azad Almasov

Yadav Nath

Yukun Yan

Department of Petroleum Engineering

Petroleum Engineering Program

APRIL 2018

TABLE OF CONTENTS

Page

ABSTRACT

Overview of subject matter: Analysis of stress concentration around wellbore for different wellbore inclination and accounting for the effect of time for a new well drilled after production from an old well which affect far field stresses due to influence of stress path.

Method of analysis: The pressure transient analytical solution using interference well is used to evaluate pore pressure at different times, using horizontal poison's ratio values. The resulting pore pressure values are used to calculate new far-field stresses using concept of stress path. The new far-field stresses are applied to a new wellbore for different wellbore inclinations after performing coordinate transformation and applying Kirsch Solutions for plane strain assumptions in cylindrical coordinate system. The principal stresses at the bore-hole wall are evaluated and is assessed based on Griffith criteria for tensile fracture and Mohr-Coulomb criteria for shear failure. The study inspects the effect of time and wellbore inclination on stress concentration for cases of reservoir depletion. Also, further investigation has been done for cases of tripping in drill string. The reservoir formation is assumed to have majorly unconsolidated sand.

Findings*:*

For isotropic far field stresses, the upper limit of mud-weight to prevent tensile fracture is found to decrease with increasing wellbore inclination because of change in orientation of far-field stress and overburden stress with respect to wellbore surface from inclination angle 0 to 90 degrees. The lower limit of mud-weight increases with increasing wellbore inclination due to the same reason. Since tectonic forces are not considered, the far-field stresses are only a small fraction (Poison's ratio) of the overburden stress.

For Isotropic far field stresses the upper limit of mud-weight increases with time because with pressure depletion due to production, the load support due to pore fluid drops and the far-field stresses thus increase; the stress required to fracture the

wellbore, thus, increases. The same applies for lower limit, the rationale being that the increasing far-field stress causing higher stress concentration at the well bore wall, resulting in more sensitive wellbore with increasing time.

For anisotropic far field stress, the behavior is similar to the isotropic case, except that since the weaker plane tends to be normal to the lower horizontal far field stress, the effect of time and inclination is seen to be more pronounced.

The difference between the allowable limits are found to increase with time due to decreased load bearing by fluid due to production, causing higher far-field stress.

The effect of depleting pore pressure can be seen in the calculated maximum and minimum horizontal stresses over time, which is found to increase.

During tripping operations, like for well logging, the pore pressure can increase for a given instant of time. This can cause borehole failure as well.

Recommendations:

The wellbore stability analysis for tight shale formation for orthotropic poison ratio stress distributions could yield better insights into the mechanics of shale formation fracking.

1. INTRODUCTION

1.1 Literature Review

Wellbore stability analysis is essential for the success of any drilling operation. This is due to the frequently encountered problems of wellbore instability and rock failures associated with drilling a hole in a field. Examples of problems include shale/clay swelling, collapse, loss circulation and unintentional formation fracturing (Last, 1995). The increasing demand for wellbore stability analyses during the planning stage of a field arises from economic considerations and the escalating use of deviated. Wellbore instability can result in lost circulation (**Figure 1-1(a)**) where tensile failure has occurred, and spalling and hole closure (**Figure 1-1(b)**) in the case of open hole section. The causes of instability are often classified into either chemical or mechanical effects. Often, field instances of instability are a result of a combination of both chemical and mechanical effects (Edwards, 2002).

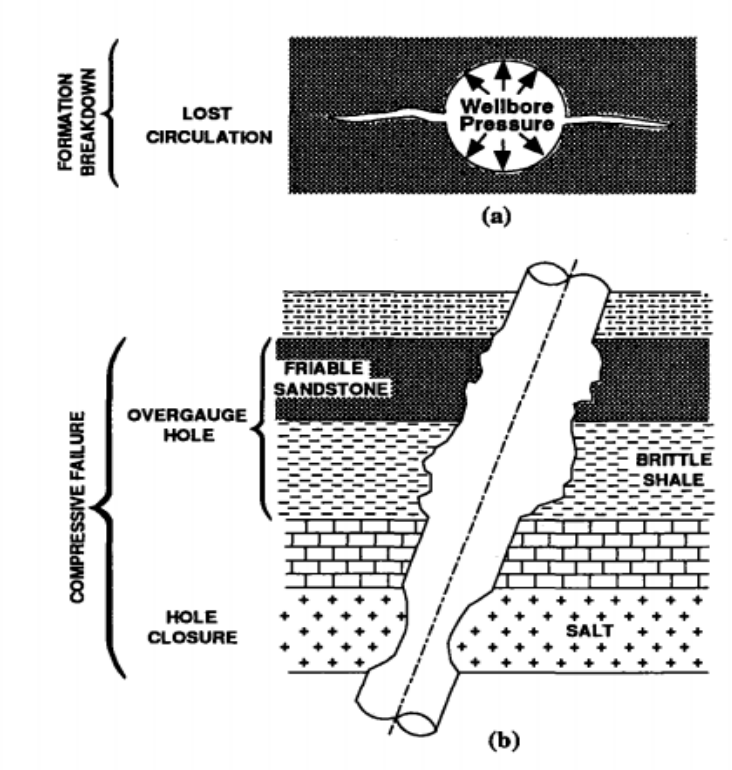

Figure 1-1. Types of stress induced wellbore instability.

Wellbore instability manifests itself in different ways like hole pack off, reaming, over pull, torque and drag, which sometimes leads to stuck pipe that may require plugging and side tracking. This requires additional time to drill a hole, driving up the cost of development. In offshore fields, loss of hole is more critical due to the limited number of holes that can be drilled from a platform (Labenski, 2003).

The two main elements required in a wellbore stability model are the failure criterion and the constitutive behavior model (Steinar, 2010).

Before a well is drilled, compressive stress exists within the rock formations (**Figure 1-2**). The stresses can be resolved into a vertical or overburden stress, S_{vert}, and two horizontal stresses, S_{Hmax} (the maximum horizontal stress), and S_{Hmin} (the minimum horizontal stress), which are generally unequal. When the well is drilled, the rock stress in the vicinity of the wellbore are redistributed as the support originally offered by the drilled out rock is replaced by the hydraulic pressure of the mud. The redistributed stresses are normally referred to as the hoop stress, σ_θ, which acts circumferentially around the wellbore wall, the radial stress, σ_r, and the axial stress, σ_z, which acts parallel to the wellbore axis. In deviated wells an additional shear component, $\sigma_{\theta z}$, is generated.

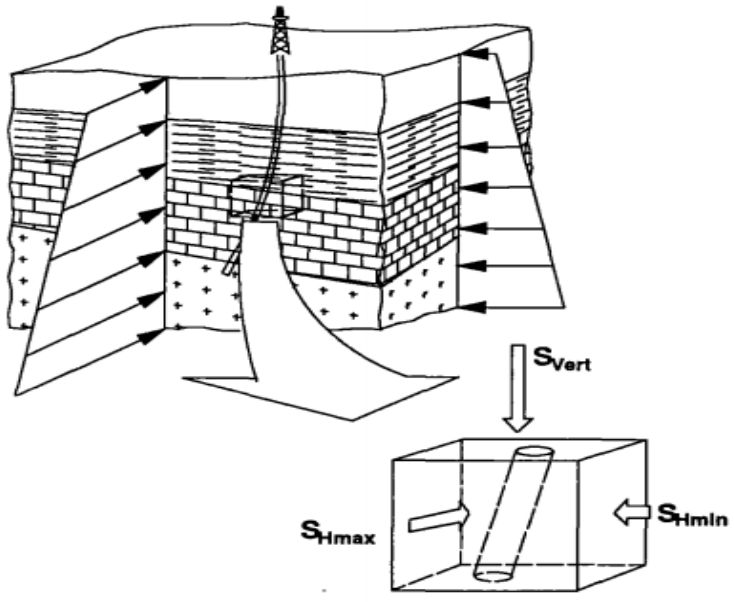

Figure 1-2. In-situ stress field.

It has been reported that wellbore instability is caused mainly by mechanical factors. Conventional approaches for the wellbore instability events, such as switching to oil-

based mud (OBM) or high-salinity water-based mud (WBM) to combat suspected reactive, water-sensitive shales has not worked; neither has the increase of mud weight in some tight hole, or shale spalling situations.

1.2 Strength Criterion

In a purely elastic analysis the stresses are compared against a peak-strength criterion normally defined in terms of the principal stresses. In an elasto-plastic analysis, plastic strains are developed once the stress state reaches a yield criterion, which in the case of perfect-plasticity coincides with the peak-strength criterion (Bradley, 1979).

An elasto-plastic analysis of wellbore stability is more realistic than a simple elastic analysis, since rocks rarely behave in a purely elastic manner up to ultimate failure. However, specifying the allowable extent of the plastic deformation before instability occurs, is difficult and somewhat arbitrary (M.R. McLean, 1990).

In case where well defined rock properties are obtained from lab testing of core, more sophisticated numerical analyses incorporating non-linear anisotropic material behavior may be performed to evaluate wellbore stability, however, in the majority of cases, the poor definition of input parameters (in-situ stress and strengths) only justifies a simple elastic analysis at best. In these cases, rock failure is determined using a peak-strength criterion. The peak-strength criterion can be determined directly from lab testing (if core is available) or from back analysis of hole conditions recorded from caliper and drilling logs (bearing in mind that this assumes a knowledge of the in-situ stresses, and the likely stress concentration around the hole).

A number of different strength criteria are commonly used to predict the onset of rock failure and wellbore instability. These criteria fall into one of the four categories (A, B, C and D) shown in **Table 1-1**.

Table 1-1. Categorization of Peak-Strength Criterion.

	Function of σ_1, σ_2 & σ_3	Function of σ_1 & σ_3 only
Linear Criterion	**Category A** e.g. Drucker-Prager [4]	**Category B** e.g. Mohr-Coulomb
Non-Linear Criterion	**Category C** e.g. Pariseau [5]	**Category D** e.g. Hoek-Brown [6]

1.3 Effect of the Intermediate Stress

The intermediate principal stress would appear to have some effect on rock strength as seen in true triaxial testing. It is informative to check various strength criteria against the two stress paths (i.e. uniaxial and biaxial). For strength criteria which fall into categories B&D, Table 1-1, the uniaxial and biaxial strength are the same. For criteria which fall into Categories A&C, the difference is often extreme which presents strength data. The data has been converted from a $\sigma_1 - \sigma_3$ stress space to a $\tau_{oct} - \sigma_{oct}$ stress space where τ_{oct} and σ_{oct} are defined as:

$$\tau_{oct} = \frac{1}{3}\sqrt{(\sigma_1 - \sigma_2)^2 + (\sigma_2 - \sigma_3)^2 + (\sigma_3 - \sigma_1)^2}$$

$$\sigma_{oct} = \frac{\sigma_1 + \sigma_2 + \sigma_3}{3}$$

The biaxial strength predicted by the failure envelope exists outside the range of the experimental data. However, from the extrapolation the predicted biaxial strength is like to be around six times the uniaxial strength, which appears excessive in the light of the previous discussion.

Nakken et al and Marsden et al express their criteria in terms of the q-p stress space as used in critical state soil mechanics.

These stress invariants are defined as:

$$q = \sigma_1 - \sigma_3$$

$$p = \frac{\sigma_1 + \sigma_2 + \sigma_3}{3}$$

For standard triaxial testing (where $\sigma_2 = \sigma_3$) the general form of p can be expresses as

$$p = \frac{\sigma_1 + 2\sigma_3}{3}$$

Figure 1-3 and **1-4** show the strength criteria given in q-p space for clay stones tested by Nakken et al and Marsden et al. For this stress space, the predicted biaxial strengths are approximately 10 and 20 times the uniaxial strengths, respectively.

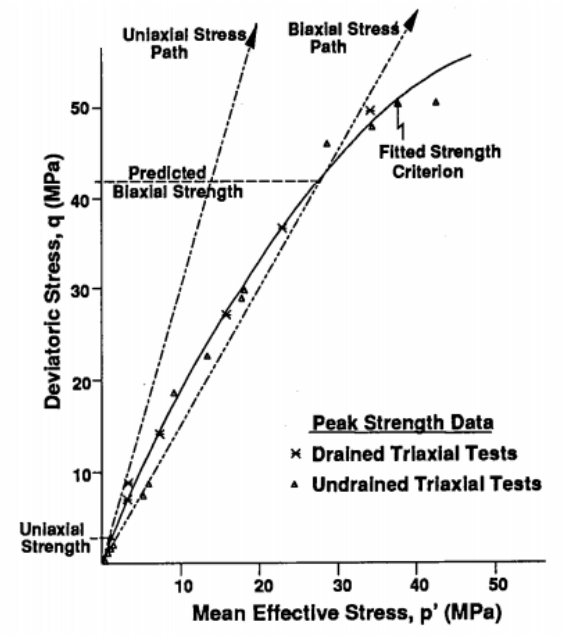

Figure 1-3. Peak-Strength Data for Weald Clay (after Nakken et al).

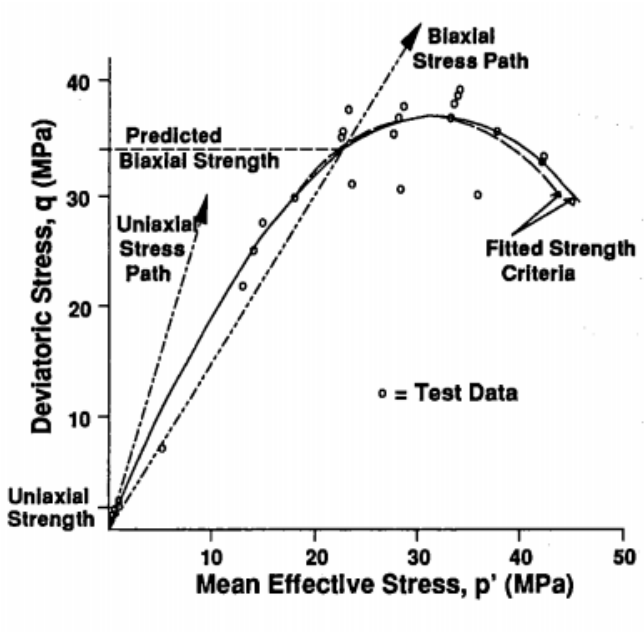

Figure 1-4. Peak-Strength Data for Weald Clay (after Marsden et al).

1.4 Constitutive Model

The main purpose of using a constitutive model is to determine the stress state around a wellbore. **Table 1-2** summaries these models. The models assume homogeneity and isotropy unless stated (Woodland, 1988).

Table 1-2. Selection of Wellbore Stability Models.

Source	Basic Model Behaviour	Additional Features
Bradley [13]	Linear Elasticity	
Paslay & Cheatham [22]	Linear Elastic	Allowance for fluid flow
Aadnøy [23]	Linear Elastic	Allowance for elastic anisotropy
Westergaard [24]	Elasto-plastic	
Veeken et al [25]	Elasto-plastic	Incorporates hardening and softening behaviour
Sulem & Vardoulakis [26]	Rigid-plastic, strain-hardening	
Santarelli [17]	Stress dependent elasticity	Includes pre-peak yielding

Given a strength criterion expressed in terms of σ_1 and σ_3, it is known from lab testing that small diameter borehole In rock are far stronger than predicted by a linear-elastic analysis. It is generally thought that wellbores are also stronger than predicted by linear-elasticity.

1.5 Wellbore Stability in Fractured Rock

Numerous wellbore instability problems related to drilling though potential fractured formation have been reported. Often, these rocks are characterized by the abundance of macro and micro scale bedding planes and networks of natural fractures. The presence of fractures weakens the rock mechanically and produces potentially higher-permeability fluid-flow paths within the low-permeability rock matrix. Practically, it is difficult to identify fracture size and fracture density without a costly core sample (Steinar, 2010).

Geomechanical simulation of instability problems requires that the input data, especially the mechanical properties are close to those of in-situ values, these properties are obtained from sonic and density logs. The properties thus obtained, called dynamic properties, have to be calibrated using those obtained in the laboratory. Through several studies it is now known that the static properties are more representative for modeling the rock in-situ stresses. Therefore, the industry standard method is to calibrate the dynamic properties calculated using sonic logs with the static measurements on cores. The industry has relied on the simple regression technique to calibrate sonic log derived mechanical properties with static measurements.

1.6 Borehole Fluid and Pressure Diffusion Mechanisms

There is a potential for borehole fluid and pressure diffusion into the near wellbore region of the rock when the bore hole pressure exceeds the formation pore pressure, if the rock has sufficient permeability, this fluid and pressure diffusion may increase the rock matrix pore pressure. This will lead to instability if the corresponding reduction in the effective normal stresses causes the resultant shear stress to intersect with the rock failure envelope. In the case of low permeable fractured shale, pressure and fluid diffusion into the fracture network may occur. In this case, the rock matrix pore pressure is nor altered but loss of effective radial stress of individual rock fragments may lead to instability.

1.7 Elasticity

Stress is tensor, therefore, operations in this study are almost always in matrix basis. There are some important concepts regarding elasticity. One of the most important concept is principal stress concept. Normally we know that stress is symmetric tensor and it has 6 components, 3 of which are perpendicular components of tractions on each surface of the material. However, other components are acting parallel to those surfaces. There is a planes of material exposed to only normal stresses only. These stresses are called principal stresses and the planes are named as principal planes. Using those stresses, we establish Mohr's circle which is very important in elasticity, poroelasticity etc. (Figure 1.1). In Figure 1.1 *S* is shear stress, *N* is normal stress (Pei Chi Chou and Nicholas J. Pagano, 1992).

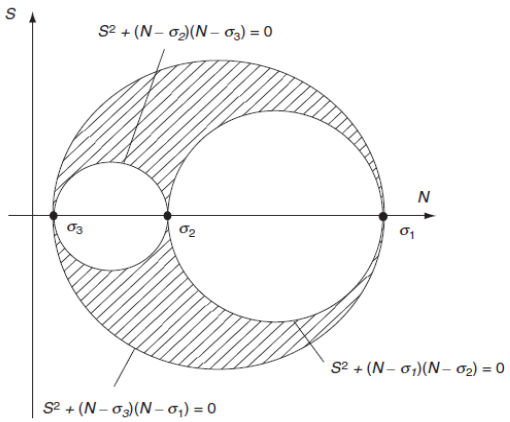

Figure 1.1: Mohr's circle for 3 dimensional case *(Sadd, 2009)*.

The stress—strain behavior of an *elastic material* during "loading" is the same as during "unloading" (J. C. Jaeger, N. G. W. Cook, R. W. Zimmerman, 2007).

1.8 Main Laws and Equations in Linear Elasticity

In this section only the names and definitions of main laws and equations are mentioned. For detailed equations and derivations one need to check the references mentioned.

Compatibility equations

We can relate strains each other with six equations which are called **compatibility equations** (Pei Chi Chou and Nicholas J. Pagano, 1992):

$$\frac{\partial^2 \varepsilon_y}{\partial z^2} + \frac{\partial^2 \varepsilon_z}{\partial y^2} = 2\frac{\partial^2 \varepsilon_{zy}}{\partial y\,\partial z} \tag{1}$$

$$\frac{\partial^2 \varepsilon_x}{\partial y^2} + \frac{\partial^2 \varepsilon_y}{\partial x^2} = 2\frac{\partial^2 \varepsilon_{xy}}{\partial x\,\partial y} \tag{2}$$

$$\frac{\partial^2 \varepsilon_x}{\partial z^2} + \frac{\partial^2 \varepsilon_z}{\partial x^2} = 2\frac{\partial^2 \varepsilon_{xz}}{\partial x\,\partial z} \tag{3}$$

$$\frac{\partial^2 \varepsilon_x}{\partial y\,\partial z} = \frac{\partial^2 \varepsilon_{xz}}{\partial x\,\partial y} + \frac{\partial^2 \varepsilon_{xy}}{\partial x\,\partial z} - \frac{\partial^2 \varepsilon_{zy}}{\partial x^2} \tag{4}$$

$$\frac{\partial^2 \varepsilon_y}{\partial x\,\partial z} = \frac{\partial^2 \varepsilon_{xy}}{\partial y\,\partial z} + \frac{\partial^2 \varepsilon_{yz}}{\partial y\,\partial z} - \frac{\partial^2 \varepsilon_{xz}}{\partial y^2} \tag{5}$$

$$\frac{\partial^2 \varepsilon_z}{\partial x\,\partial y} = \frac{\partial^2 \varepsilon_{xz}}{\partial y\,\partial z} + \frac{\partial^2 \varepsilon_{yz}}{\partial x\,\partial z} - \frac{\partial^2 \varepsilon_{xy}}{\partial z^2} \tag{6}$$

Principle of superposition

This principle states that two strain field may be combined by direct superposition. It creates possibilities to isolate displacement due to pure deformation and rotation at any point in the linear theory (Pei Chi Chou and Nicholas J. Pagano, 1992).

Hooke's law

$$\varepsilon_x = \frac{1}{2G}\sigma_x - \frac{\nu}{E}\sigma_{kk} \tag{7}$$

$$\varepsilon_y = \frac{1}{2G}\sigma_y - \frac{\nu}{E}\sigma_{kk} \tag{8}$$

$$\varepsilon_z = \frac{1}{2G}\sigma_z - \frac{\nu}{E}\sigma_{kk} \tag{9}$$

$$\varepsilon_{xy} = \frac{\tau_{xy}}{2G} \tag{10}$$

$$\varepsilon_{yz} = \frac{\tau_{yz}}{2G} \tag{11}$$

$$\varepsilon_{xz} = \frac{\tau_{xz}}{2G} \tag{12}$$

Where:

$$\sigma_{kk} = \sigma_x + \sigma_y + \sigma_z \tag{13}$$

Equilibrium equations

$$\frac{\partial \sigma_{xx}}{\partial x} + \frac{\partial \sigma_{xy}}{\partial y} + \frac{\partial \sigma_{xz}}{\partial z} + B_x = 0 \tag{14}$$

$$\frac{\partial \sigma_{xy}}{\partial x} + \frac{\partial \sigma_{yy}}{\partial y} + \frac{\partial \sigma_{yz}}{\partial z} + B_y = 0 \tag{15}$$

$$\frac{\partial \sigma_{xz}}{\partial x} + \frac{\partial \sigma_{yz}}{\partial y} + \frac{\partial \sigma_{zz}}{\partial z} + B_z = 0 \tag{16}$$

Where, B_x, B_y, B_z are body forces in *x, y, z* directions respectively (Miska, Handout #1A - Fundamental Concepts of Elasticity, 2017).

Using equations above Beltrami-Mitchell and Lame equations can be derived which are very important for linear elasticity problems.

1.9 Poroelasticity

The equations and laws stated above is correct for almost all materials. In porous medium the linear elasticity is different. First of all at very little stress changes due to micro fractures inside rock stress-strain relationship is not linear. However, it becomes linear after some point. Using superposition principle stated above, we can look at the strain in the bulk as two kind of strains. Strains of grains due to hydrostatic pressure (which is equal to confining pressure in unjacketed test), and strains due to loading of the dry porous media by the stresses $\sigma_{x,y,z}$ +P (here due to sign convention we wrote +P, where P pore pressure taken as negative). After applying superposition and Hooke's law we can derive Hooke's law for porous media:

$$\varepsilon_x = \frac{1+\nu_B}{E_B}\sigma_x - \frac{3\nu_B}{E_B}\overline{\sigma} + \left(\frac{1}{K_B} - \frac{1}{K_M}\right)\frac{P}{3} \tag{17}$$

$$\varepsilon_y = \frac{1+\nu_B}{E_B}\sigma_y - \frac{3\nu_B}{E_B}\overline{\sigma} + \left(\frac{1}{K_B} - \frac{1}{K_M}\right)\frac{P}{3} \qquad (18)$$

$$\varepsilon_z = \frac{1+\nu_B}{E_B}\sigma_z - \frac{3\nu_B}{E_B}\overline{\sigma} + \left(\frac{1}{K_B} - \frac{1}{K_M}\right)\frac{P}{3} \qquad (19)$$

Where, K_B, K_M are bulk and matrix modulus respectively. Defining effective stress, we could rewrite Hooke's law:

$$\varepsilon_x = \frac{1+\nu_B}{E_B}\sigma_{xeff} - \frac{3\nu_B}{E_B}\overline{\sigma}_{eff} \qquad (20)$$

$$\varepsilon_y = \frac{1+\nu_B}{E_B}\sigma_{yeff} - \frac{3\nu_B}{E_B}\overline{\sigma}_{eff} \qquad (21)$$

$$\varepsilon_z = \frac{1+\nu_B}{E_B}\sigma_{zeff} - \frac{3\nu_B}{E_B}\overline{\sigma}_{eff} \qquad (22)$$

When,

$$\sigma_{xeff} = \sigma_x + \alpha P \qquad (23)$$

$$\sigma_{yeff} = \sigma_y + \alpha P \qquad (24)$$

$$\sigma_{zeff} = \sigma_z + \alpha P \qquad (25)$$

$$\overline{\sigma}_{eff} = \sigma_{meff} = \overline{\sigma} + \alpha P \qquad (26)$$

Where,

$$\alpha = 1 - \frac{K_B}{K_M} \qquad (27)$$

All in all, the main equations can be summed up as:

Pure compliance formulation

$$\varepsilon_{kk} = \varepsilon_{vol} = \varepsilon = \frac{1}{K}\overline{\sigma} + \frac{\alpha}{K}P \qquad (28)$$

$$\zeta = \frac{\Delta M}{V\rho_o} = \frac{\alpha}{K}\overline{\sigma} + \frac{\alpha}{KB}P \qquad (29)$$

Pure stiffness formulation

$$\overline{\sigma} = K_u\varepsilon_{kk} - (K_u B)\zeta \qquad (30)$$

$$P = -(K_u B)\varepsilon_{kk} + \left(\frac{K_u B}{\alpha}\right)\zeta \qquad (31)$$

$$K_u = \frac{\delta\bar{\sigma}}{\delta\varepsilon_{kk}} = \frac{K}{1-\alpha B} \qquad (32)$$

Where, K_u is undrained bulk modulus. Drained test is the test where pore pressure is kept constant whereas undrained test is the test where fluid exit is not allowed.

Mixed stiffness formulation

$$\bar{\sigma} = K\varepsilon_{kk} - \alpha P \qquad (33)$$

$$\zeta = \alpha\varepsilon_{kk} + \left(\frac{\alpha}{K_u B}\right) P \qquad (34)$$

Mixed compliance formulation

$$\varepsilon_{kk} = \frac{\bar{\sigma}}{Ku} + B\zeta \qquad (35)$$

Where, ζ is fluid increment, B is Skempton's coefficient which relates fluid increment with strain (actually fluid and bulk strains) at constant mean stress ($\bar{\sigma}$) (Miska, Handout#2 - Poroelasticity, 2017).

General Procedure for orienting far-field stress along well-bore coordinates:

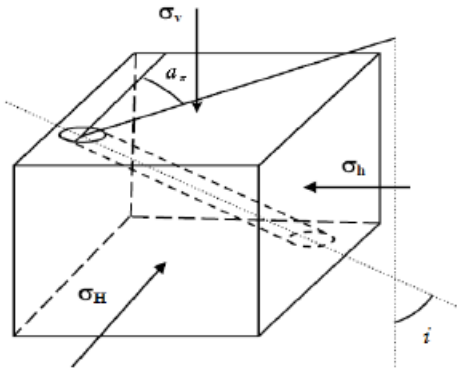

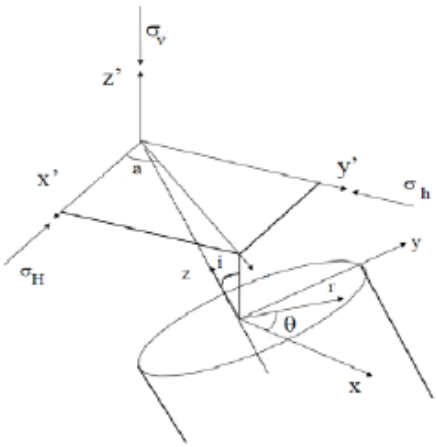

Far-field stresses on reservoir:

$$[\sigma]_{x'y'z'} = \begin{bmatrix} \sigma_H & 0 & 0 \\ 0 & \sigma_h & 0 \\ 0 & 0 & \sigma_v \end{bmatrix}$$

The transformation of stresses:

- A rotation of a around the z'-axis.
- A rotation of i around the (new) y'-axis.

The transformation of stress:

- A rotation of ‘ a ’ about z’ axis:

$$T_1 = \begin{bmatrix} \cos a & \sin a & 0 \\ -\sin a & \cos a & 0 \\ 0 & 0 & 1 \end{bmatrix}$$

- A rotation of ‘ i ‘ about y’ axis:

$$T_2 = \begin{bmatrix} \cos i & 0 & -\sin i \\ 0 & 1 & 0 \\ \sin i & 0 & \cos i \end{bmatrix}$$

$$L = T_2 \times T_1$$

Well-bore coordinate system in cartesian coordinates:

$$[\sigma]_{xyz} = [L][\sigma]_{x'y'z'}[L]^T$$

$$\begin{bmatrix} \sigma^o_{xx} \\ \sigma^o_{yy} \\ \sigma^o_{zz} \\ \sigma^o_{xy} \\ \sigma^o_{yz} \\ \sigma^o_{xz} \end{bmatrix} = \begin{bmatrix} l^2_{xx'} & l^2_{xy'} & l^2_{xz'} \\ l^2_{yx'} & l^2_{yy'} & l^2_{yz'} \\ l^2_{zx'} & l^2_{zy'} & l^2_{zz'} \\ l_{xx'}l_{yx'} & l_{xy'}l_{yy'} & l_{xz'}l_{yz'} \\ l_{yx'}l_{zx'} & l_{yy'}l_{zy'} & l_{yz'}l_{zz'} \\ l_{zx'}l_{xx'} & l_{zy'}l_{xy'} & l_{zz'}l_{xz'} \end{bmatrix} \begin{bmatrix} \sigma_H \\ \sigma_h \\ \sigma_v \end{bmatrix}$$

$$l_{xx'} = \cos a \cos i; \quad l_{xy'} = \sin a \cos i; \quad l_{xz'} = -\sin i$$

$$l_{yx'} = \cos a \cos i; \quad l_{yy'} = \sin a \sin i; \quad l_{yz'} = 0$$

$$l_{zx'} = \cos a \sin i; \quad l_{zy'} = \sin a \sin i; \quad l_{zz'} = \cos i$$

Expanding:

$$\sigma_x^0 = \left(\sigma_H \cos^2 a + \sigma_h \sin^2 a\right)\cos^2 i + \sigma_v \sin^2 i$$

$$\sigma_y^0 = \sigma_H \sin^2 a + \sigma_h \cos^2 a$$

$$\sigma_z^0 = \left(\sigma_H \cos^2 a + \sigma_h \sin^2 a\right)\sin^2 i + \sigma_v \cos^2 i$$

$$\sigma_{xy}^0 = \tau_{xy} = \frac{1}{2}\left(\sigma_h - \sigma_H\right)\sin 2a \cos i$$

$$\sigma_{xz}^0 = \tau_{xz} = \frac{1}{2}\left(\sigma_H \cos^2 a + \sigma_h \sin^2 a - \sigma_v\right)\sin 2i$$

$$\sigma_{yz}^0 = \tau_{yz} = \frac{1}{2}\left(\sigma_h - \sigma_H\right)\sin 2a \sin i$$

It is preferable to use cylindrical coordinate system of well-bore stress as opposed to cartesian coordinates:

The expressions for the independent stress components in the cylindrical coordinate system are listed as follows:

$$\sigma_{rr} = \left(\frac{\sigma_{xx}^o + \sigma_{yy}^o}{2}\right)\left(1 - \frac{r_w^2}{r^2}\right) + \left(\frac{\sigma_{xx}^o - \sigma_{yy}^o}{2}\right)\left(1 + 3\frac{r_w^4}{r^4} - 4\frac{r_w^2}{r^2}\right)\cos 2\theta + \sigma_{xy}^o\left(1 + 3\frac{r_w^4}{r^4} - 4\frac{r_w^2}{r^2}\right)\sin 2\theta + P_w\frac{r_w^2}{r^2}$$

$$\sigma_{\theta\theta} = \left(\frac{\sigma_{xx}^o + \sigma_{yy}^o}{2}\right)\left(1 + \frac{r_w^2}{r^2}\right) - \left(\frac{\sigma_{xx}^o - \sigma_{yy}^o}{2}\right)\left(1 + 3\frac{r_w^4}{r^4}\right)\cos 2\theta - \sigma_{xy}^o\left(1 + 3\frac{r_w^4}{r^4}\right)\sin 2\theta - P_w\frac{r_w^2}{r^2}$$

$$\sigma_{zz} = \sigma_{zz}^o - \nu\left[2\left(\sigma_{xx}^o - \sigma_{yy}^o\right)\frac{r_w^2}{r^2}\cos 2\theta + 4\sigma_{xy}^o\frac{r_w^2}{r^2}\sin 2\theta\right]$$

$$\sigma_{r\theta} = \left(\frac{\sigma_{xx}^o - \sigma_{yy}^o}{2}\right)\left(1 - 3\frac{r_w^4}{r^4} + 2\frac{r_w^2}{r^2}\right)\sin 2\theta + \sigma_{xy}^o\left(1 - 3\frac{r_w^4}{r^4} + 2\frac{r_w^2}{r^2}\right)\cos 2\theta$$

$$\sigma_{\theta z} = \left(-\sigma_{xz}^o \sin\theta + \sigma_{yz}^o \cos\theta\right)\left(1 + \frac{r_w^2}{r^2}\right)$$

$$\sigma_{rz} = \left(\sigma_{xz}^o \cos\theta + \sigma_{yz}^o \sin\theta\right)\left(1 - \frac{r_w^2}{r^2}\right)$$

For the deviated wellbore solution,

@ wellbore, $r = R_w$

$$\sigma_r = P_w$$

$$\sigma_\theta = \sigma_x^o + \sigma_y^o - 2(\sigma_x^o - \sigma_y^o)\cos 2\theta - 4\tau_{xy}^0 \sin 2\theta - P_w$$

$$\sigma_z = \sigma_z^o - \nu_B\left[2(\sigma_x^o - \sigma_y^o)\cos 2\theta + 4\tau_{xy} \sin 2\theta\right]$$

$$\tau_{r\theta} = 0$$

$$\tau_{\theta z} = 2(-\tau_{xz}^0 \sin\theta + \tau_{yz}^0 \cos\theta)$$

$$\tau_{rz} = 0$$

In order to find the principal stress at the borehole wall:

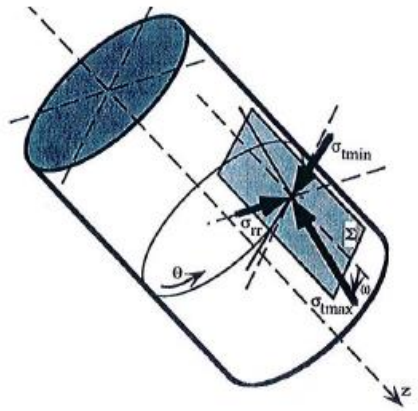

$$\sigma_1 = \sigma_{t\max} = \frac{1}{2}\left[\sigma_z + \sigma_\theta + \sqrt{(\sigma_z - \sigma_\theta)^2 + 4\tau_{\theta z}^2}\right]$$

$$\sigma_2 = \sigma_{t\min} = \frac{1}{2}\left[\sigma_z + \sigma_\theta - \sqrt{(\sigma_z - \sigma_\theta)^2 + 4\tau_{\theta z}^2}\right]$$

$$\sigma_3 = \sigma_r = \Delta P$$

The angle ω can be calculated as follows:

$$\tan 2\omega = \frac{2\tau_{\theta z}}{\sigma_z - \sigma_\theta}$$

WHY DOES PORE PRESSURE CHANGE?

1. Due to drill-out, there is stress re-distribution, and there is **volumetric strain**; this effect does not require the well-bore to be penetrated.
2. Communication of wellbore bore with formation pressure during **production.**

After drill-out or wellbore pressure change, **stress redistribution**:

- Non-porous linear elastic material: Immediate
- *Porous, permeable medium*: ***Time delayed effect***

The borehole wall is permeable. This means:

- We $\mathbf{P_w}$ instead of $\mathbf{P_f}$ while computing effective stress using Terzaghi's failure formula:

$$\sigma' = \sigma - p_f$$

and remaining part of the total stresses are carried by the pore fluid.

$$\sigma'_r = 0$$

Note: this equation is based on ***plane strain assumption***; *well-bore is very long*.

- Breakout or compression failure:

  Applying Mohr-Coulomb Criterion, using terizaghi's failure formula ($\alpha = 1$) for:

  $\sigma_\theta > \sigma_z > \sigma_r$

$$\sigma'_\theta = C_o + \sigma'_r \tan^2 \beta$$

$$p_{w,min} = \frac{2\sigma_h - 2\eta p_{fo} - C_0}{2 - 2\eta} = \frac{2\sigma_h - \alpha\frac{1-2\nu_{fr}}{1-\nu_{fr}} p_{fo} - C_0}{2 - \alpha\frac{1-2\nu_{fr}}{1-\nu_{fr}}}$$

- Hydraulic fracturing criteria:
  - Vertical Fracturing:

    $\sigma'_\theta = -T_0$

$$p^{frac}_{w,max} = \frac{2\sigma_h - 2\eta p_{fo} + T_0}{2 - 2\eta} = \frac{2\sigma_h - \alpha\frac{1-2\nu_{fr}}{1-\nu_{fr}} p_{fo} + T_0}{2 - \alpha\frac{1-2\nu_{fr}}{1-\nu_{fr}}}$$

  - Horizontal Fracturing:

    $\sigma'_z = -T_0.$

$$p^{frac}_{w,max} = \frac{\sigma_v - 2\eta p_{fo} + T_0}{1 - 2\eta} = \frac{\sigma_v - \alpha\frac{1-2\nu_{fr}}{1-\nu_{fr}} p_{fo} + T_0}{1 - \alpha\frac{1-2\nu_{fr}}{1-\nu_{fr}}}$$

1.10 Generalized Diffusivity Equations

After having introduced poroelasticity now we can apply it to the equations playing main role in reservoir engineering. The most important equation in reservoir engineering is diffusivity equation. Till recent years, in reservoir engineering, the geo-mechanical properties of rocks haven't been considered in diffusivity equations etc. We can include well-testing to this list as well. Recent studies have shown that these properties (PR, Young modulus etc.) have considerable effect on reservoir performance and reservoir flow regimes predictions, especially in unconventional reservoirs.

Fracture conductivity depends on fracture orientation when anisotropy of the geo-mechanical properties is considered. Anisotropy of Young's Modulus and Poisson's Ratio shows vital effect on fracture mechanics (Mark McGinley, Ding Zhu, and A. Daniel Hill, 2015). Different assumptions can be considered during derivation of general diffusivity equation.

Finally, using plain strain approach, diffusivity equation has been developed as the following:

$$P(r,t) = P_i + \frac{141.2q\mu}{kh}Ei\left(-\frac{r^2}{4\varsigma t}\right) \qquad 36$$

$$\varsigma = \frac{6.328\,k}{\mu(\emptyset C_t)_p}$$

where,

$$S = (\emptyset C_t)_p = -\frac{2}{3}\frac{(C_b - C_s)^2}{C_b}\frac{1-2v}{1-v} + \emptyset C - (1+\emptyset)C_s + C_b$$

2. STATEMENT OF THE PROBLEM

As mentioned above mud window (minimum and maximum mud weight) can change with time. There could be a lot of reason for it. The collapse of a borehole, however, is sometimes found to be time-delayed; that is, not happening at the time of the drilling, but at some later time. While this delay can be attributed to a number of factors, such viscoelastic creep and chemical reaction of shale, poroelastic effects certainly play an important role (Alexandre H. and D. Cheng, 2016).

However, we also know that during production of the reservoir, pore pressure changes. As pore pressure changes far field stresses are changing due to pressure induced stress path. This, as a result, affect wellbore stability, therefore, our wellbore stability become time-dependent.

In this project, only the effect of the pore pressure changes on wellbore stability is investigated.

3. SOLUTION OF THE PROBLEM

In introduction section, wellbore stability equations using Mohr-Columb criterion, were introduced. In those equations, if we replace far field stresses by stress path equations for Orthotropic condition (anisotropic case) we can easily relate our wellbore stability equations to the pore pressure. But we need assumptions as the following:

- Plane of the symmetry is assumed to be the same

$$\begin{cases} \upsilon_{xy} = \upsilon_{yx} = \upsilon_{h} \\ \upsilon_{zx} = \upsilon_{xz} = \upsilon_{vmin} \\ \upsilon_{zy} = \upsilon_{yz} = \upsilon_{vmax} \end{cases}$$

- The same Young's modulus and Biot's coefficient in all directions
- Plane strain diffusivity solution for pressure
- Impermeable wellbore (undrained condition)
- Linear elastic deformations
- Isotropic and homogenous formation

- Fully penetrating vertical well
- Axi-symmetric condition, $\partial\partial\theta(\ldots)=0$
- Single-Phase fluid
- Constant permeability
- Constant fluid viscosity
- Horizontal fluid flow (purely radial flow)
- Irrotational displacement field
- Zero body forces
- Uniform variation along the z-direction, $\partial\partial z(\ldots)=\text{const}$
- Constant vertical stress
- While drilling second well in not-virgin reservoir, we assume that pore pressure doesn't change with time (that is, our first production well shut in)
- Ignore viscoelastic properties of the rock

3.1 Solution Procedure

Step 1. After these assumptions our equations become as the following

$$\frac{\Delta\sigma_h}{\Delta P} = -\alpha\left(1 - \frac{\nu_{vmin} + \nu_h \nu_{vmax}}{1 - \nu_h{}^2}\right)$$

$$\frac{\Delta\sigma_H}{\Delta P} = -\alpha\left(1 - \frac{\nu_{vmin}\nu_h + \nu_{vmax}}{1 - \nu_h{}^2}\right)$$

Step 2. In stress path equations instead of pore pressure difference, we use plain strain line source solution equation for pressure given in the introduction part.

$$P(r,t) = P_i + \frac{141.2q\mu}{kh}\,Ei\left(-\frac{r^2}{4\varsigma t}\right)$$

where,

$$\varsigma = \frac{6.328\,k}{\mu(\emptyset C_t)_p} \qquad S = (\emptyset C_t)_p = -\frac{2}{3}\frac{(C_b - C_s)^2}{C_b}\frac{1-2\nu}{1-\nu} + \emptyset C - (1+\emptyset)C_s + C_b$$

Here ν is horizontal Poisson's ratio – ν_h which can be obtained from well test data.

Step 3. Transform farfield stresses to inclined well xyz coordinate system using the transformation matrices for inclination and azimutal orientation. Resulted stress equations are the followings:

$$\sigma_x^0 = (\sigma_H \cos^2 a + \sigma_h \sin^2 a)\cos^2 i + \sigma_v \sin^2 i$$
$$\sigma_y^0 = \sigma_H \sin^2 a + \sigma_h \cos^2 a$$
$$\sigma_z^0 = (\sigma_H \cos^2 a + \sigma_h \sin^2 a)\sin^2 i + \sigma_v \cos^2 i$$
$$\sigma_{xy}^0 = 0.5 * (\sigma_h - \sigma_H)\sin 2a \cos i$$
$$\sigma_{xz}^0 = 0.5 * (\sigma_H \cos^2 a + \sigma_h \sin^2 a - \sigma_v)\sin 2i$$
$$\sigma_{yz}^0 = 0.5 * (\sigma_h - \sigma_H)\sin 2a \sin i$$

Step 4. Then we show the independent stress components in the cylindrical coordinate system including wellbore pressure for r = Rw:

$$\sigma_{rr} = P_w$$
$$\sigma_{\theta\theta} = (\sigma_x^0 + \sigma_y^0) - 2(\sigma_x^0 - \sigma_y^0)\cos 2\theta - 4\sigma_{xy}^0 \sin 2\theta - P_w$$
$$\sigma_{zz} = \sigma_z^0 - \nu_B[2(\sigma_x^0 - \sigma_y^0)\cos 2\theta + 4\sigma_{xy}^0 \sin 2\theta]$$
$$\tau_{r\theta} = 0$$
$$\tau_{\theta z} = 2(-\sigma_{xz}^0 \sin\theta + \sigma_{yz}^0 \cos\theta)$$
$$\tau_{rz} = 0$$

Step 5. Now we need to find maximum and minimum principal stresses. I have to mention that for different criteria (fracture and collapse) our maximum and minimum principal stresses will change. We know that on r face since there is not any tangential stresses ($\tau_{r\theta} = \tau_{rz} = 0$), $\sigma_{rr} = Pw$ automatically is the principal stress, which will be

in the middle between 1 and 3 (Remember the Mohr's circle for 3D: we have three faces, therefore we will have 3 Mohr's circle and three principal stresses). We will use different Mohr's circles, both of which are inside the big circle, for different criteria. That means I will look at the principal stress at different faces for different criteria. For fracture:

$$\sigma_1 = P_w$$
$$\sigma_3 = \frac{1}{2}(\sigma_\theta + \sigma_z) - \frac{1}{2}\sqrt{(\sigma_\theta - \sigma_z)^2 + 4\tau_{\theta z}^2}$$

The borehole will fracture at the minimum effective minimal principal stress equal to the tensile strength : $\sigma_3' = \sigma_3 - \alpha P_{pore} = T$

Using the equation for σ_3 inside the equation above we can derive the expression for the σ_θ: $\sigma_\theta = \frac{\tau_{\theta z}^2}{\sigma_z - T - \alpha P_{pore}} + \alpha P_{pore} + T$

And, using the expression for the σ_θ we can easily derive the equation for the maximum mud weight that will result fracture at the bottomhole:

$$P_{wf} = \sigma_x + \sigma_y - 2(\sigma_x - \sigma_y)\cos 2\theta - 4\tau_{xy}\sin 2\theta - \frac{\tau_{\theta z}^2}{\sigma_z - T - \alpha P_{pore}} - \alpha P_{pore} - T$$

However, we know that the first fracture will start in the direction of higher principal stress. Further increasing of bottomhole pressure will result fracture in other directions. However, we need to find the pressure at which the first fracture will start. Therefore, we will find the minimum fracture pressure. From calculus we know that to find minimum of the function we need to take its derivative and equal to zero. Therefore, the equation will be differentiated w.r.t θ to find the direction (minimum fracture pressure). For in case I have signed this angel as θ_{min} to differentiate from others in the Matlab code provided in Appendix A after the conclusion part:

$$\theta = \frac{1}{2}\arctan\frac{2\tau_{xy}}{\sigma_x - \sigma_y}$$

So, using this radial angle in the equation provided for Pwf we can find the maximum bottomhole pressure which will cause fracture in the direction of this angle. And using the equation below I have calculated maximum mud weight in ppg: $\rho_{max} = \frac{P_{wf}}{0.052 * D}$

Step 6. For collapse principal stresses are as following:

$$\sigma_1 = \frac{1}{2}(\sigma_\theta + \sigma_z) + \frac{1}{2}\sqrt{(\sigma_\theta - \sigma_z)^2 + 4\tau_{\theta z}^2}$$
$$\sigma_3 = P_w$$

And, using the Mohr-Coulumb criteria given below:

$$\frac{1}{2}(\sigma_1' - \sigma_3')\cos\phi = S_0 + \left[\frac{1}{2}(\sigma_1' + \sigma_3') - \frac{1}{2}(\sigma_1' - \sigma_3')\sin\phi\right]\tan\phi$$

As you see we will need to solve this equation for every given radial angle and inclination angle to solve for collapse pressure-P_{wc}, and since this equation is non-linear for P_{wc} we will need to use iteration. However, since we know that collapse happens then θ = 90. Therefore, I have used Newton-Raphson iteration solve for P_{wc} for θ equal to 90 degrees, and for every inclination angle. After all I have calculated minimum mud density which will cause collapse. All results are tabulated and plotted for different cases in the following section

So, finally, one can make this statement that during production pore pressure changes; then because of stress path horizontal stresses changes with time; therefore, principal stresses changes with time.

It has to be mentioned that in this project only production induced wellbore stability during time has been taken into consideration. However, future study can be done for drilling induced wellbore stability, creeping etc.

In this project, different inclination angles also have been taken into the consideration as well as isotropy and anisotropy cases.

Applying those steps I have developed code in the Matlab given in Appendix A using the input data given in the following model.

3.2 Model

Reservoir model parameters and geomechanic parameters for this project has been tabulated in the Table 1 as our base case.

Table 1: Base case reservoir parameters

Depth (ft)	9482	Cs-solid compressibility (1/psi)	1.81E-07
degree of internal friction	42.4	Cb-bulk compressibility (s/psi)	8.62E-07
degree of azimuth	10	Cw-water compressibility (1/psi)	2.86E-06
gradient (psi/ft)	1	qw- flow rate (STB/D)	2734
Biot's coefficient	1	h-reservoir thickness (ft)	160
cohesive strength (psi)	1182	rr- observation distance (ft)	327
Initial pore pressure-Pi (psi)	3500	Bw-FVF of water (bbl/STB)	1
v_h (horizontal poisson's ratio)	0.382	mu-viscosity of water (cP)	1.16
v_vmin (minimum vertical poissons ratio)	0.2	sigma_h0-minimum horizontal stress) (psi)	6143
v_vmax (maximum vertical poissons ratio)	0.35	sigma_H0-maximum horizontal stress) (psi)	7500
T_0 - tensile strength (psi)	0	t-production time (years)	50

Reservoir parameters has been taken from the paper-SPE-166074 ((Mojtaba P. Shahri and Stefan Z. Miska, 2015 October).

3.3 Results

For isotropy case, both horizontal stresses have been taken as 6143 psi; $\nu_{vmin} = \nu_{vmax} = \nu_h = 0.382$. For anisotropy case σ_h=6143 psi; σ_H=7500 psi; ν_{vmin} =0.2; ν_{vmax} =0.35; ν_h= 0.382.

Different inclination angles are taken from 0 to 90 degree. Production time has been divided into 5 logarithmic steps, since in the beginning reservoir pressure decline sharply.

For different times maximum mud weight and minimum mud weight vs inclination angle output data is plotted (Figures 1 and 2).

Table 2: Results for Case 1 (isotropic case).

Case 1	time (years)									
inc_deg	0.01		0.084089642		0.707106781		5.946036		50	
	mw_min	mw_max	mw_min	mw_max	mw_min	mw_max	mw_min	mw_max	mw_min	mw_max
0.1	7.16	18.34	7.10	18.53	7.03	18.72	6.97	18.91	6.90	19.10
5.1	7.30	18.29	7.24	18.48	7.19	18.67	7.13	18.86	7.08	19.04
10.1	7.52	18.14	7.46	18.33	7.41	18.52	7.35	18.71	7.30	18.90
15.1	7.75	17.89	7.69	18.09	7.64	18.28	7.58	18.47	7.53	18.66
20.1	7.99	17.56	7.94	17.76	7.88	17.95	7.83	18.14	7.77	18.34
25.1	8.24	17.15	8.18	17.35	8.13	17.55	8.07	17.74	8.01	17.94
30.1	8.49	16.68	8.43	16.88	8.37	17.08	8.32	17.28	8.26	17.48
35.1	8.73	16.15	8.67	16.36	8.61	16.57	8.56	16.77	8.50	16.98
40.1	8.97	15.60	8.91	15.81	8.85	16.02	8.79	16.23	8.73	16.44
45.1	9.19	15.02	9.13	15.24	9.07	15.45	9.01	15.67	8.95	15.88
50.1	9.39	14.45	9.33	14.67	9.27	14.89	9.21	15.10	9.15	15.32
55.1	9.58	13.89	9.52	14.11	9.45	14.34	9.39	14.56	9.33	14.79
60.1	9.74	13.37	9.68	13.60	9.62	13.82	9.56	14.05	9.49	14.28
65.1	9.88	12.90	9.82	13.13	9.76	13.36	9.70	13.59	9.63	13.82
70.1	10.00	12.49	9.94	12.72	9.87	12.96	9.81	13.19	9.75	13.43
75.1	10.09	12.16	10.03	12.40	9.96	12.64	9.90	12.87	9.84	13.11
80.1	10.16	11.92	10.09	12.16	10.03	12.40	9.97	12.64	9.90	12.88
85.1	10.19	11.77	10.13	12.01	10.07	12.25	10.00	12.49	9.94	12.73
90	10.21	11.72	10.14	11.96	10.08	12.20	10.02	12.45	9.95	12.69

Table 3: Results for Case 2

Case 2	time (years)									
inc_deg	0.01		0.084089642		0.707106781		5.946036		50	
	mw_min	mw_max	mw_min	mw_max	mw_min	mw_max	mw_min	mw_max	mw_min	mw_max
0.1	8.25	15.63	8.21	15.83	8.17	16.03	8.13	16.24	8.09	16.44
5.1	8.28	15.60	8.24	15.80	8.20	16.01	8.16	16.21	8.12	16.41
10.1	8.37	15.52	8.33	15.72	8.28	15.93	8.24	16.13	8.20	16.33
15.1	8.50	15.39	8.45	15.59	8.40	15.80	8.36	16.00	8.31	16.21
20.1	8.64	15.20	8.59	15.41	8.55	15.62	8.50	15.83	8.45	16.03
25.1	8.80	14.98	8.75	15.19	8.70	15.40	8.65	15.61	8.60	15.82
30.1	8.97	14.72	8.91	14.93	8.86	15.14	8.81	15.36	8.76	15.57
35.1	9.13	14.42	9.08	14.64	9.02	14.86	8.97	15.08	8.91	15.29
40.1	9.29	14.11	9.24	14.33	9.18	14.55	9.13	14.78	9.07	15.00
45.1	9.45	13.78	9.39	14.01	9.33	14.24	9.28	14.46	9.22	14.69
50.1	9.59	13.46	9.54	13.69	9.48	13.92	9.42	14.15	9.36	14.38
55.1	9.73	13.14	9.67	13.37	9.61	13.61	9.55	13.84	9.49	14.07
60.1	9.85	12.84	9.79	13.08	9.73	13.31	9.66	13.55	9.60	13.79
65.1	9.95	12.57	9.89	12.81	9.83	13.05	9.77	13.29	9.70	13.53
70.1	10.04	12.33	9.97	12.57	9.91	12.82	9.85	13.06	9.79	13.30
75.1	10.10	12.14	10.04	12.38	9.98	12.63	9.92	12.88	9.85	13.12
80.1	10.15	12.00	10.09	12.24	10.03	12.49	9.96	12.74	9.90	12.99
85.1	10.18	11.91	10.12	12.16	10.06	12.41	9.99	12.66	9.93	12.91
90	10.19	11.88	10.13	12.13	10.07	12.38	10.00	12.63	9.94	12.88

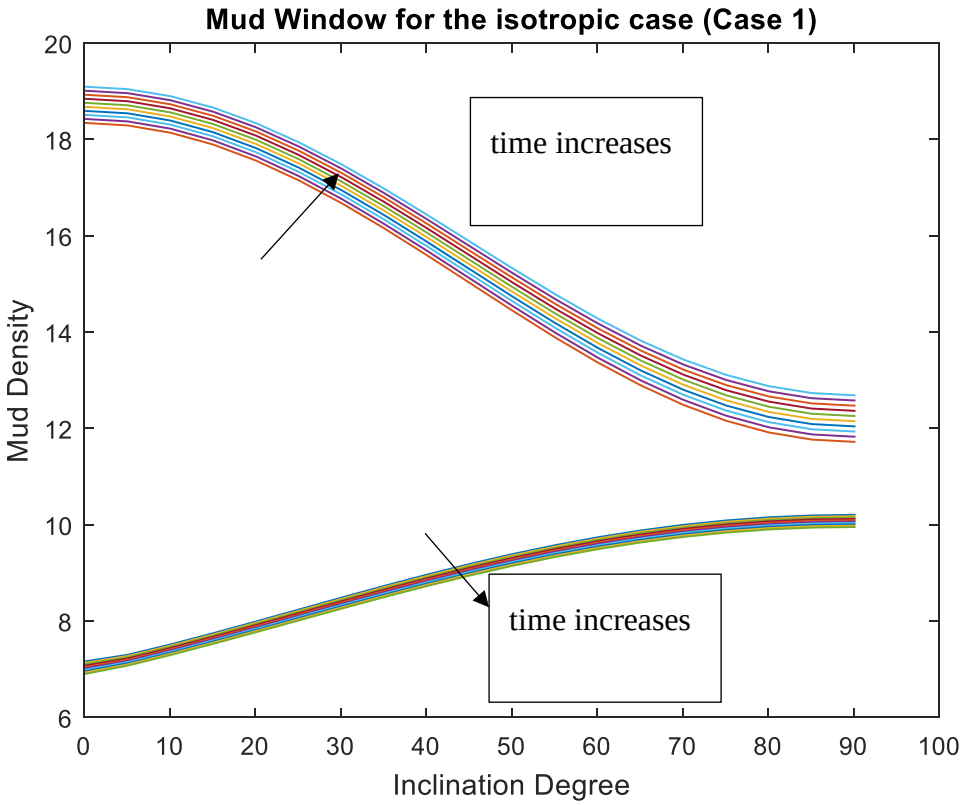

Figure 1: Results for Case 1 (isotropic case).

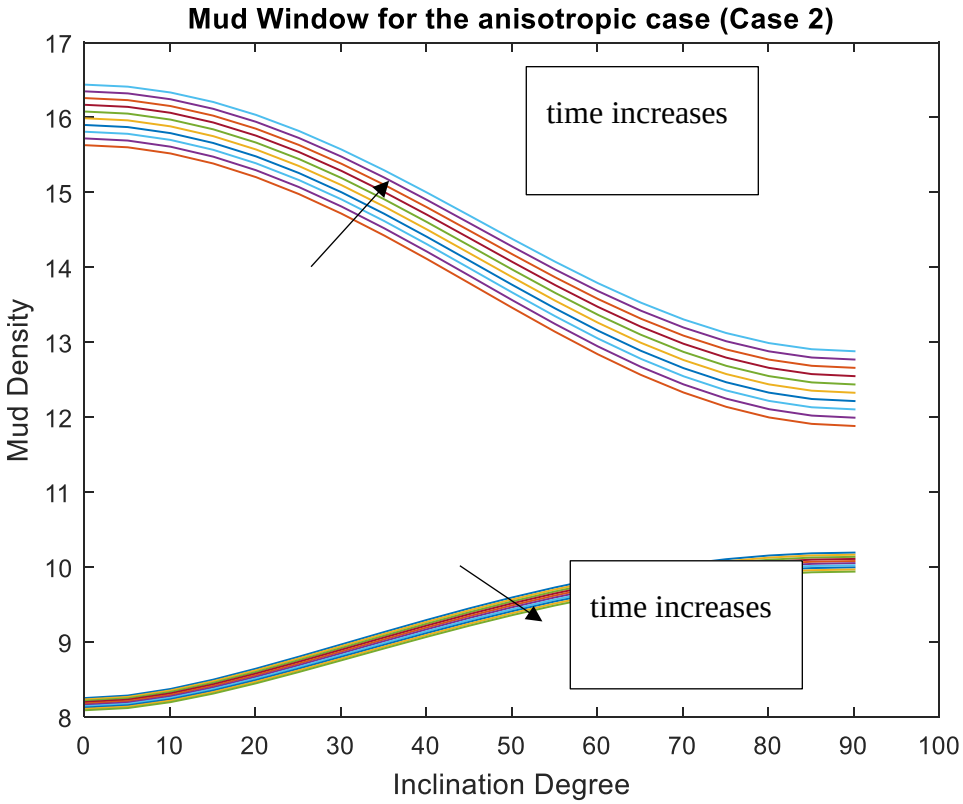

Figure 2: Results for Case 2 (anisotropic case).

I have also plotted how pore pressure as well as σ_h, σ_H, change with time for both isotropic and anisotropic cases (Figures 3 to 8).

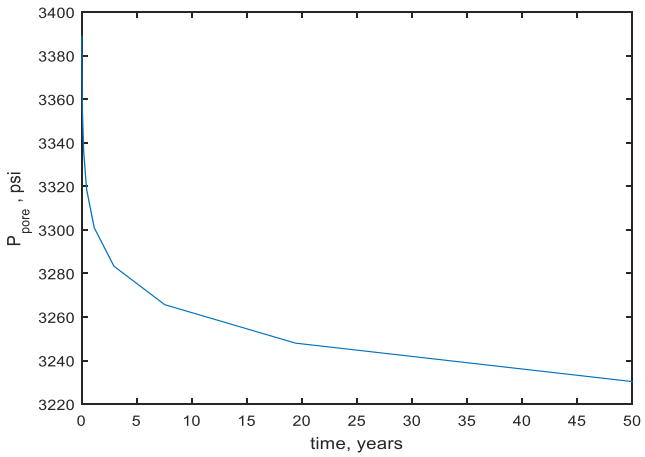

Figure 3: P_{pore} vs time in Isotropy case.

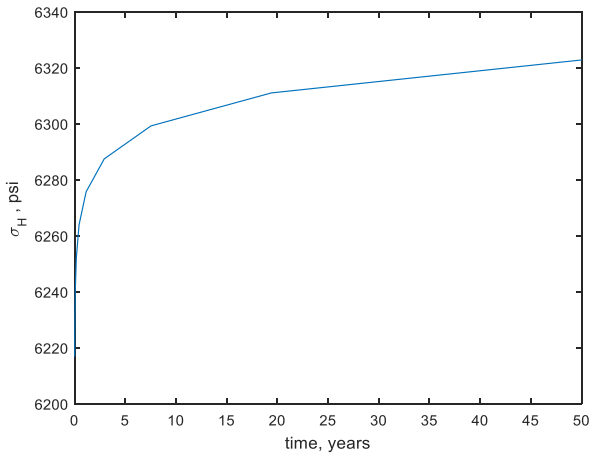

Figure 4: σ_H vs time in Isotropy case.

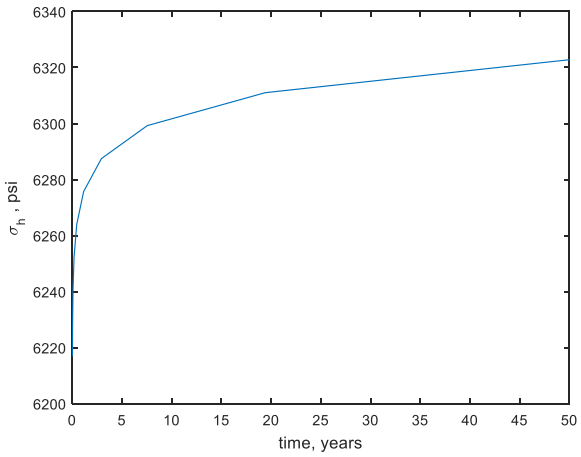

Figure 5: σ_h vs time in Isotropy case.

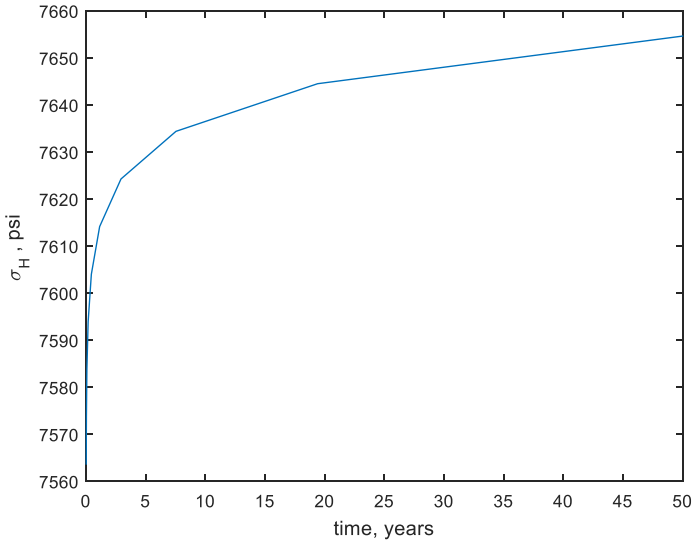

Figure 7: σ_H vs time in Anisotropy case.

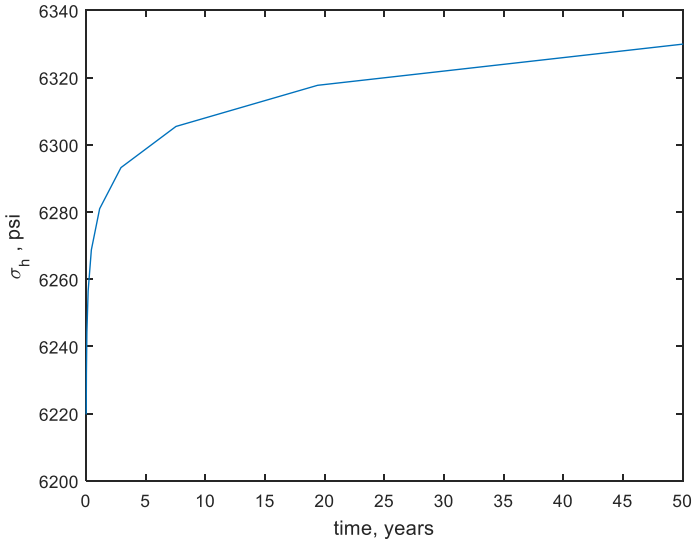

Figure 8: σ_h vs time in Anisotropy case.

From plots Figure 1 and 2 it is obvious that maximum mud weight increases with production time and minimum mud weight decreases with time. These results are reasonable because when we have lower pore pressure, we will have higher far field stresses, and thus, it will be harder to create fracture. However, we will need lower mud weight to prevent collapse. To see the effect of the time of production on mud window choice minimum and maximum mud weight differences have been plotted for vertical and horizontal wells for both anisotropy and isotropy cases (Figures 9 to 12). If we look at the far field stresses vs time plots for both cases, we will see that they follow the same trend as opposite of pore pressure changes with time.

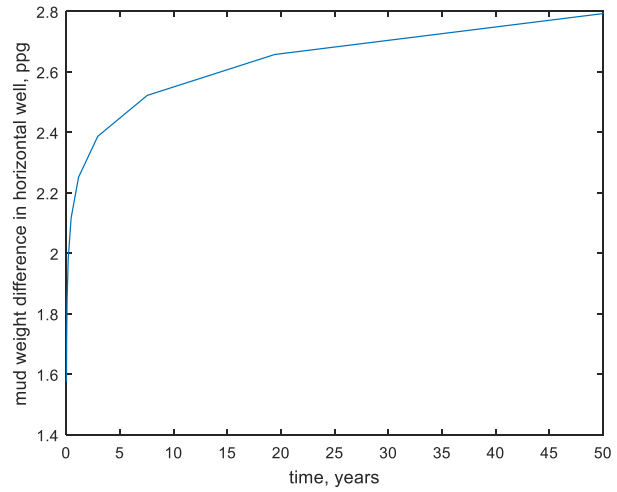

Figure 9: Mud window vs time for horizontal well in isotropy case.

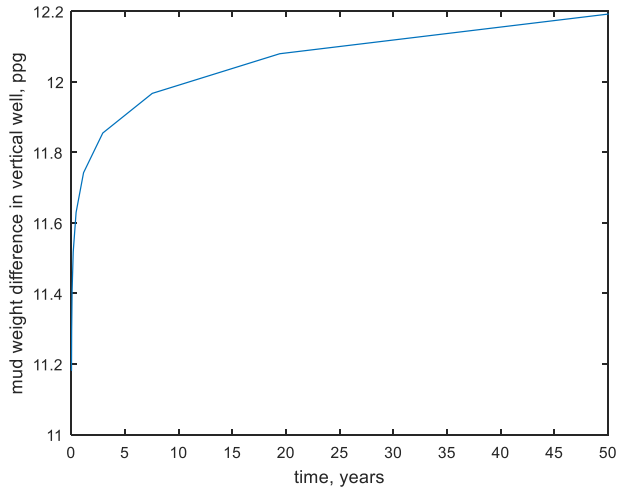

Figure 10: Mud window vs time for vertical well in isotropy case.

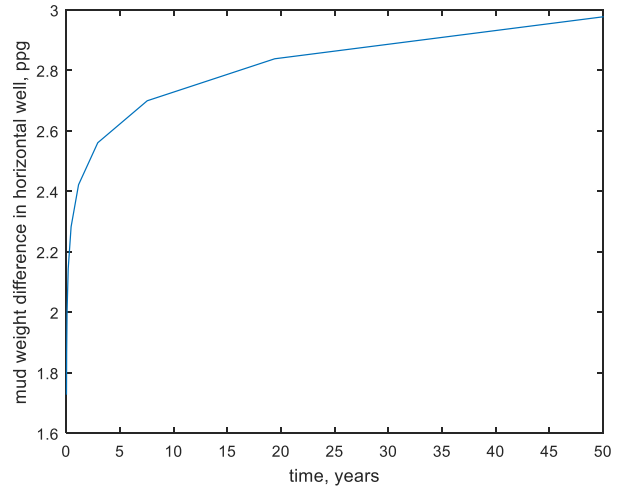

Figure 11: Mud window vs time for horizontal well in anisotropy case.

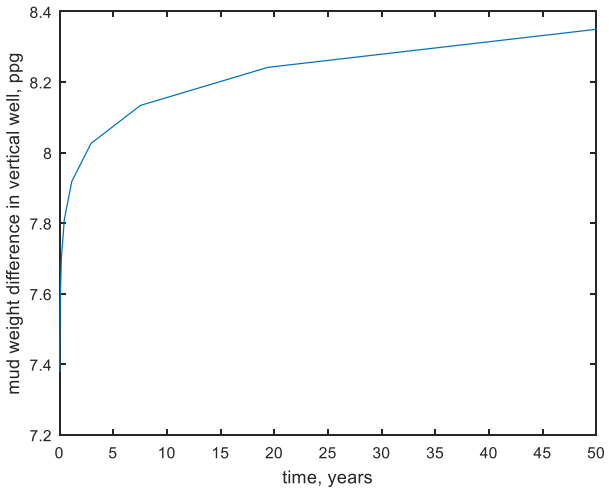

Figure 12: Mud window vs time for vertical well in anisotropy case.

Mud weight differences vs time plots follow the same trend as the far field stresses. If we look at the equations of collapse and fraction criterion we will see that this kind of similarity is reasonable.

4. STATEMENT OF THE EXTRA PROBLEM – TIME DELAYED WELLBORE FAILURE

The problem stated above is for instant time. That is, we take it into consideration when we drill new well in the reservoir that is not virgin. Most of time drillers use old geological data for far field stresses which are not the same after a production. However, as we see that is not big problem because mud window getting larger as pore pressure decreases.

However, in the field problem occurs with time during tripping and logging operations. And the reason for this is pore pressure to increase around wellbore. As a result, Mohr circle shift to the shear failure curve (Figure 13).

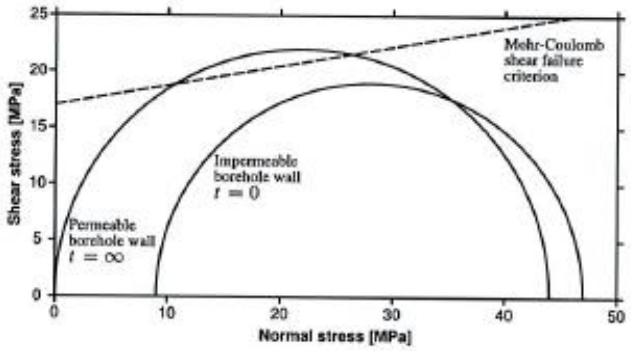

Figure 13: Time delayed Mohr circle shift.

However, I don't know how this pore pressure increases with time.

To visualize this, I assumed pore pressure build up as if we shut in the well. Therefore, I have used the same mine source equation for fully transient (infinite acting reservoir), and I have used superposition principle for shut in (build-up), that is as if we produce with negative rate.

For this purpose, all my reservoir properties are the same except the initial reservoir pressure = P_i= 3200 psi and I produce with = q_w= -2734 STB/D. I have only showed the results for anisotropy case.

5. SOLUTION OF THE EXTRA PROBLEM

I have plotted mud window vs inclination angle plot for this (Figure 14). From the figure it is obvious that this kind of failure can affect horizontal wells much more than

vertical ones. These all about how misleading choosing mud window could be if we did not consider time delayed pore pressure change etc.

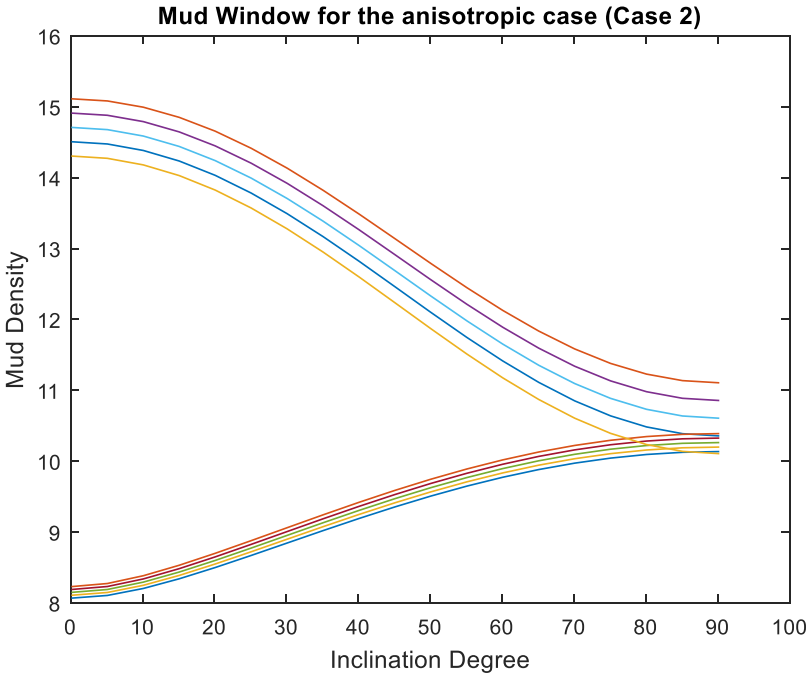

Figure 14: Mud window for anisotropy case (time delayed).

However, to check time delayed wellbore failure, I have assumed constant wellbore pressure (constant mud weight), and see how Mohr circles changes. This affect increases when we have permeable borehole. To see this, we may increase permeability, but I will not do that since it is the same procedure and it will not do anything more to get an idea. To do so, I only considered big circle where my minimum and maximum normal stresses are as following:

$$\sigma 1 = \frac{1}{2}(\sigma\theta + \sigma z) + \frac{1}{2}\sqrt{(\sigma\theta - \sigma z)^2 + 4\tau\theta z^2}$$

$$\sigma 3 = \frac{1}{2}(\sigma\theta + \sigma z) - \frac{1}{2}\sqrt{(\sigma\theta - \sigma z)^2 + 4\tau\theta z^2}$$

Resulted Mohr circles for different cases are plotted (Figures 15 to 18).

In all cases Mohr circle shift to left because of pore pressure increase. And in all cases as pore pressure increases radius of Mohr circle increases, except in the case of vertical well in anisotropic reservoir. Only in that case radius of Mohr circle decreases as it shifts to the left. To see it clear I have plotted this Radius (maximum shear stress) vs time for 4 inclination angles (0.1, 5.1, 10.1, 15.1) (Figure 16). For further inclination

angles the trend is the same as was in the last inclination angle in the Figure 16 (I=15.1).

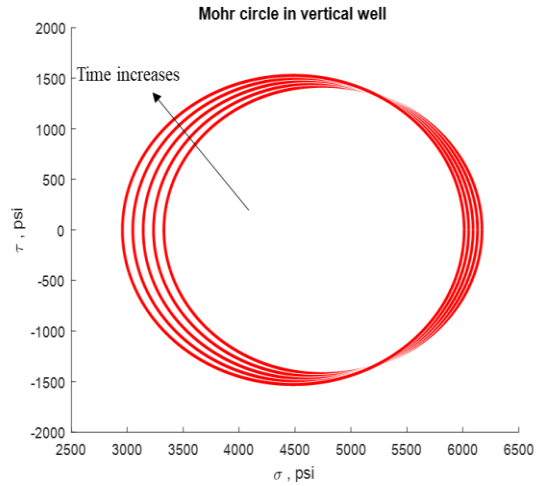

Figure 15: Mohr circle for isotropic case for vertical well.

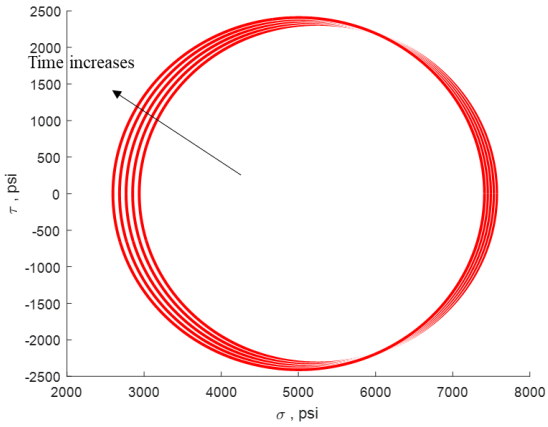

Figure 15: Mohr circle for isotropic case for 20 degree inclined well.

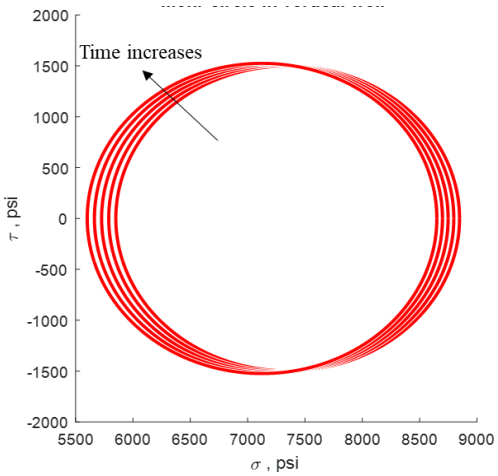

Figure 15: Mohr circle for anisotropic case for 20 degree inclined well.

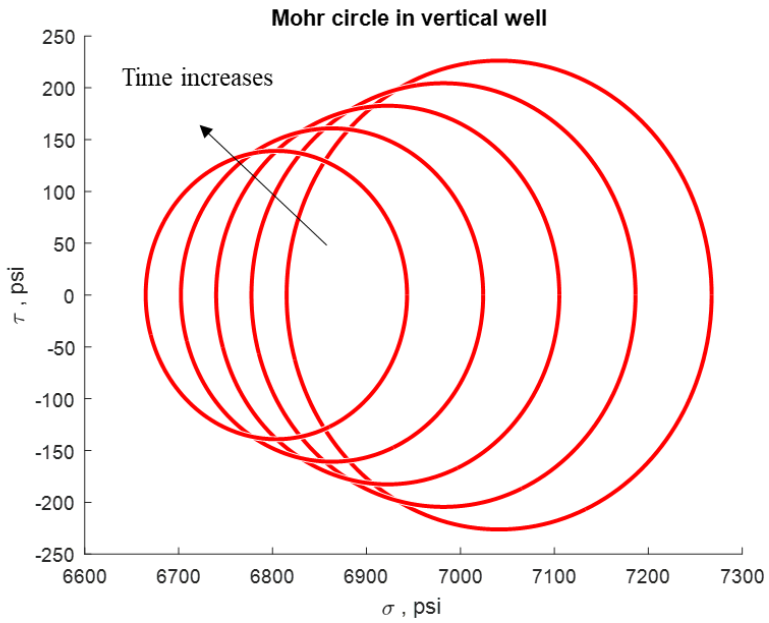

Figure 15: Mohr circle for anisotropic case for vertical well.

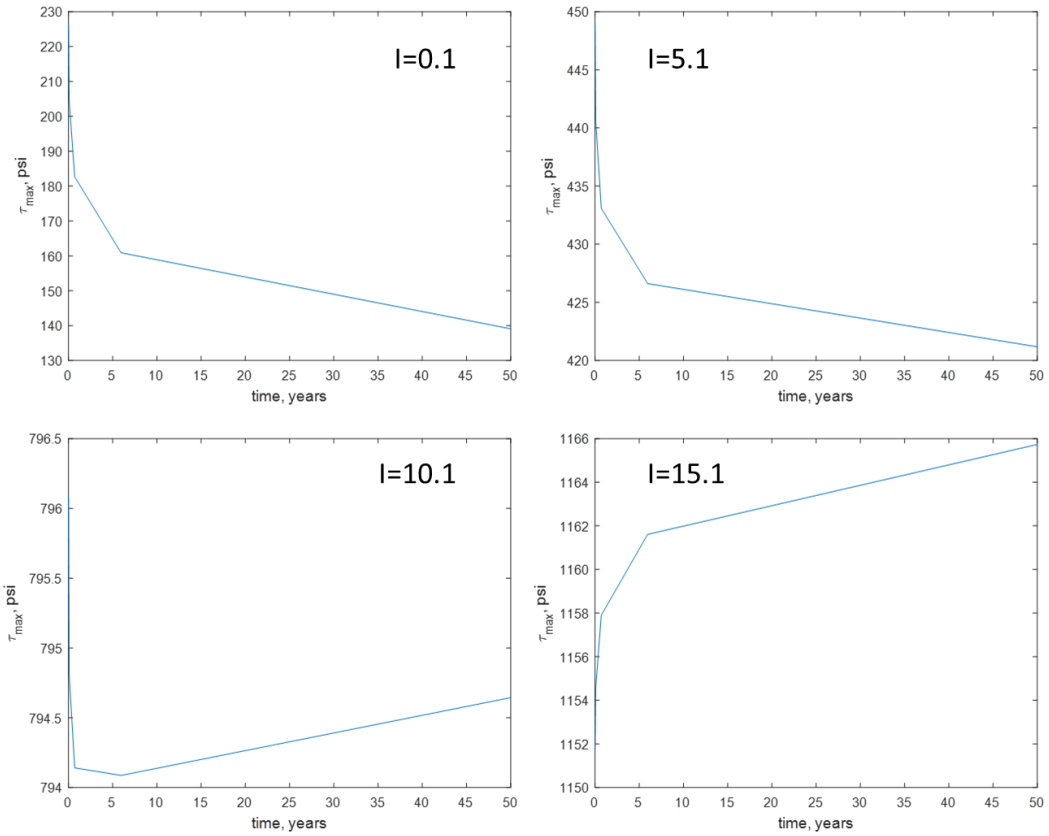

Figure 16: maximum shear stress changes with time for different inclination angles.

I don't know the reason why in the anisotropy case for lower inclination angles my code showed such result. To check my code, I have plotted σ_1' vs σ_3' for vertical well and horizontal well, which is for Mohr-Coulomb criterion has to show linear

relationship (Figure 17). As it can be seen from plots they are both linear, which means code works correctly. What can be concluded from these plots is that *uniaxial compressive strength is getting higher as inclination degree increases*.

However, since my code is working good, there should be explanation to the behavior in the Figure 16. I didn't figure it out yet and I will let it to be as future work.

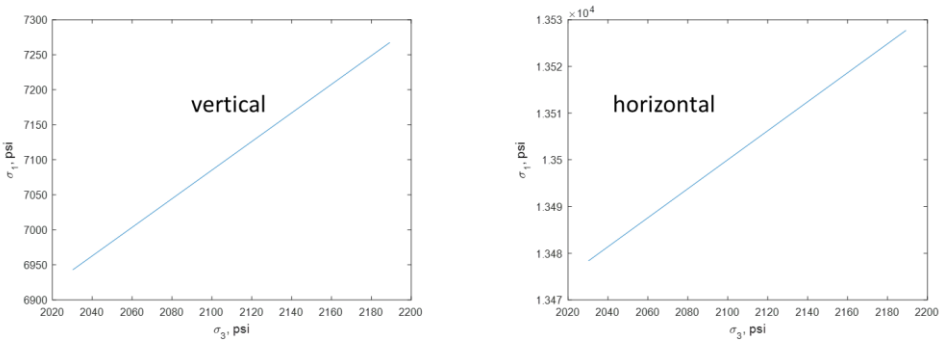

Figure 17: Checking code with Mohr-Coulomb criterion.

However, when pressure drop is high, we don't have such problem in lower inclination angles.

CONCLUSIONS

1. All criteria are for principal stresses. One can't use stresses itself to compare with criteria. Furthermore, one can't use effective stress concept for any other stresses than principal stresses, because principal stresses are the indication of the perpendicular tractions, and, because pressure is itself is perpendicular we have to use principal stresses
2. Depending on pore pressure effective stress changes, thus it affects criteria. Further work should be done to check the effect of the pore pressure of the reservoir on criteria
3. As inclination angle increases it affects mud window to get closer, which is critical issue by means of well-stability
4. The effect of difference between far field stresses decreases as inclination angle approaches to 90 degrees (horizontal well), and for horizontal well both cases were the same
5. For different far field stresses mud window was closer that of equal far field stresses. This work is obvious prove how the difference between far field stresses makes role
6. Different minimum and maximum principal stresses have to be used depending on the type of failure (fracture or collapse). This is because fracture and collapse happen different planes of the rock. To understand this better one need to establish Mohr's circle and determine principal stresses for each planes. Using r face of the figure we could end up with the biggest Mohr's circle (where is the maximum and minimum principal stresses can be derived using σ_θ and σ_{zz}) and σ_{rr} will be in between, and thus using first circle we will evaluate fracture, and using the second circle (where the minimum principal stress is σ_{rr}) we will evaluate collapse. So fracture happens perpendicular to the r face, and collapse happen perpendicular to the θ face
7. For different angle of inclination and for different point of borehole (for different θ) we have different principal

8. Pore pressure plays very important role in wellbore stability by means of stress path: pore pressure induced far field stress change
9. Production history has to be considered when we estimate mud window
10. Tripping and logging operation can cause pore pressure increase and this results in far field stresses to decrease. As a result, mud window gets narrower. This may result borehole failure
11. Uniaxial compressive strength gets higher with increasing inclination angle
12. As pore pressure increases maximum shear stress increases at all inclination angles except lower inclination angles from 0 to 15.
13. The reason why in lower inclination angle maximum shear stress is getting lower as pore pressure increases is left as future work.

BIBLIOGRAPHY

Alexandre H. and D. Cheng. (2016). *Poroelasticity* (Vol. 27). (J. Bear, Ed.) Oxford, Missisippi, USA: Springer International Publishing Switzerland.

Dong Chen, Zhejun Pan, Zhihui Ye. (2014). Dependence of the gas shale fracture permeability on effective stress and reservoir pressure: Model match and insights. *Fuel*, 383-392.

Gai, X. (2004). *A Coupled Geomechanics and Reservoir Flow Model on Parallel Computers.* PhD Thesis Dissertation , The University of Texas at Austin , Austin.

J. C. Jaeger, N. G. W. Cook, R. W. Zimmerman. (2007). *Fundamentals of Rock Mechanics* (Fourth ed.). Malden, USA: Blackwell.

Mark McGinley, Ding Zhu, and A. Daniel Hill. (2015). The Effects of Fracture Orientation and Elastic Property Anisotropy on Hydraulic Fracture Conductivity in the Marcellus Shale . *SPE, 174870*.

Miska, S. Z. (2017). *Handout #1A - Fundamental Concepts of Elasticity.* Tulsa.

Miska, S. Z. (2017). *Handout#2 - Poroelasticity.* Tulsa.

Mojtaba P. Shahri and Stefan Z. Miska. (2015 October). In-Situ Poisson's Ratio Determination from Interference Transient Well Test. *SPE*, 1041.

Mojtaba P. Shahri, Stefan Z. Misk, SPE, The University of Tulsa Drilling Research Projects. (2013). In-Situ Poisson's Ratio Determinationfrom Interference Transient Well Test. *SPE*.

Pei Chi Chou and Nicholas J. Pagano. (1992). *Elasticity: Tensor, Dyadic & Engineering Approaches.* Princeton, New Jersey: Nostrand Company, Inc.

S. Baldino, S. Rafiepoor, and S. Z. Miska. (2017, March 31). In-Situ Poisson's Ratio Determination under Different Deformational Conditions. *SPE*.

Sadd, M. H. (2009). Elasticity: Theory, Applications, and Numerics. In M. H. Sadd, *Elasticity: Theory, Applications, and Numerics* (p. 63). Burlington, MA 01803, USA: Elsevier Inc.

Willson, K. (2015). Analysis of Drawdown Sensitivity in Shale Reservoirs Using Coupled-Geomechanics Models. *SPE*.

Edwards, S.T., Matsutsuya, B. and Willson,S.M. 2002. Imaging unstable wellbores while drilling, Paper SPE 79846 presented at the SPE ATCE, San Antonio, Texas, USA, 29 Sepyember-2 October.

Labenski, F., Reid, P. and Santos, H. 2003. Drilling Fluids Approaches for Control of Wellbore Stability in Fractured Formations. Paper SPE/IADC 85304 presented at the SPE/IADC Middle East Drilling Technology Conference and Exhibition, Abu Dabi, UAE, 20-22 October.

Last, N.G, Plumb, R., Harknessm R., Charlez, P., Alsen, J., and McLean, M. 1995. An Integrated Approach to Evaluating and Managing Wellbore Instability in the Cusiana Field, Colombia, South American. Paper SPE 30464 presented at the SPE ATCE, Dallas, TX, USA, 22-25 October.

Steinar Ottesen. 2010. Wellbore Stability in Fractured Rock. Paper SPE/IADC 128728 presented at SPE/IADC Drilling Conference and Exhibition, New Orleans, Louisiana, USA, 2-4 February.

Woodland, D.C. 1988. Borehole Instability in the Western Canadian Overthrust Belt. SPE rocky mountain regional meeting, Casper, Wy, May.

Bradley, W. B. 1979. Mathematical Stress Cloud - Stress Cloud can Predict Borehole Failure. Oil and Gas J., Vol.77, No.8, Feb., pp.92-102.

M. R. McLean and M. A. Addis. 1990. Wellbore Stability Analysis: A Review of Current Methods of Analysis and Their Field Application. Paper SPE/IADC 19941 presented at the SPE/IADC Drilling Conference and Exhibition, Houston, Taxas, USA, 27 February -2 March.

ADDENDUM – CONTRIBUTIONS OF EACH STUDENTS

Each student did the following things:

Azad Almasov: Developed Matlab code; Statement of the Problem; Solution of the Problem; Extra Problem; Solution of the Extra Problem; Conclusions

Yadav Nath: Introduction (Literature review); Abstract; Conclusions

Yukun Yan: Introduction (Literature review).